Engineering Out Motion: A Surface Disulfide Bond Alters the Mobility of Tryptophan 22 in Cytochrome b_5 As Probed by Time-Resolved Fluorescence and ^{1}H NMR Experiments†

Elizabeth M. Storch, Jeffrey S. Grinstead, A. Patricia Campbell, Valerie Daggett, and William M. Atkins*

Department of Medicinal Chemistry, University of Washington, Box 357610, Seattle, Washington 98195-7610

Received September 8, 1998; Revised Manuscript Received February 2, 1999

ABSTRACT: In the accompanying paper [Storch et al. (1999) *Biochemistry 38*, 5054−5064] equilibrium denaturation studies and molecular dynamics (MD) simulations were used to investigate localized dynamics on the surface of cytochrome b_5 (cyt b_5) that result in the formation of a cleft. In those studies, an S18C:R47C disulfide mutant was engineered to inhibit cleft mobility. Temperature- and urea-induced denaturation studies revealed significant differences in Trp 22 fluorescence between the wild-type and mutant proteins. On the basis of the results, it was proposed that wild type populates a conformational ensemble that is unavailable to the disulfide mutant and is mediated by cleft mobility. As a result, the solvent accessibility of Trp 22 is decreased in S18C:R47C, suggesting that the local environment of this residue is less mobile due to the constraining effects of the disulfide on cleft dynamics. To further probe the structural effects on the local environment of Trp 22 caused by inhibition of cleft formation, we report here the results of steady-state and time-resolved fluorescence quenching, differential phase/modulation fluorescence anisotropy, and ^{1}H NMR studies. In Trp fluorescence experiments, the Stern−Volmer quenching constant increases in wild type versus the oxidized disulfide mutant with increasing temperature. At 50 °C, K_{SV} is nearly 1.5-fold greater in wild type compared to the oxidized disulfide mutant. In the reduced disulfide mutant, K_{SV} was the same as wild type. The bimolecular collisional quenching constant, k_q, for acrylamide quenching of Trp 22 increases 2.7-fold for wild type and only 1.8-fold for S18C:R47C, upon increasing the temperature from 25 to 50 °C. The time-resolved anisotropy decay at 25 °C was fit to a double-exponential decay for both the wild type and S18C:R47C. Both proteins exhibited a minor contribution from a low-amplitude fast decay, consistent with local motion of Trp 22. This component was more prevalent in the wild type, and the fractional contribution increased significantly upon raising the temperature. The fast rotational component of the S18C:R47C mutant was less sensitive to increasing temperature. A comparison of the ^{1}H NMR monitored temperature titration of the δ-methyl protons of Ile 76 for wild type and oxidized disulfide mutant, S18C:R47C, showed a significantly smaller downfield shift for the mutant protein, suggesting that Trp 22 in the mutant protein experiences comparatively decreased cleft dynamics in core 2 at higher temperatures. Furthermore, comparison of the δ'-methyl protons of Leu 25 in the two proteins revealed a difference in the ratio of the equilibrium heme conformers of 1.2:1 for S18C:R47C versus 1.5:1 for wild type at 40 °C. The difference in equilibrium heme orientations between wild type and S18C:R47C suggests that the disulfide bond affects heme binding within core 1, possibly through damped cleft fluctuations. Taken together, the NMR and fluorescence studies support the proposal that an engineered disulfide bond inhibits the formation of a dynamic cleft on the surface of cyt b_5.

Cytochrome b_5 (cyt b_5)[1] plays a critical role in reductive and oxidative metabolism of endogenous substrates and xenobiotics. Redox partners of the microsomal membrane-bound form of cyt b_5 include several cytochrome P450s, cytochrome P450 reductase, and stearyl-CoA desaturase (*1*, *2*), whereas mitochondrial cyt b_5 interacts with cyt b_5 reductase and cyt *c* (*3*). In addition, nonredox roles for cyt b_5 have been suggested, in which cyt b_5 acts as an allosteric effector. For example, apocyt b_5 stimulates the metabolism of several drugs by cytochrome P450 3A4 (*4*, *5*), and holocyt b_5 alters the metabolite production of cytochrome P450c17 (*6*, *7*). The versatility of cyt b_5 and its ability to interact with such a wide range of structurally diverse partners have prompted the suggestion that multiple conformations may contribute to its function.

Solubilized cyt b_5 consists of two cores (Figure 1). Core 1 includes the heme cofactor inserted into a α-helix bundle,

† Supported by the National Institutes of Health (GM 50789 to V.D.) and the Department of Medicinal Chemistry (to W.M.A. and A.P.C.).

* To whom correspondence should be addressed. Phone: (206) 685-0379. FAX: (206) 685-3252. E-mail: winky@u.washington.edu.

[1] Abbreviations: cyt b_5, cytochrome b_5; MD, molecular dynamics; S18C:R47C$_{ox}$, oxidized S18C:R47C; S18C:R47C$_{red}$, reduced and acetylated S18C:R47C; NMR, nuclear magnetic resonance; MALDI-TOF; matrix-assisted laser desorption ionization time-of-flight; λ_{mass}, spectral center of mass; K_{SV}, Stern−Volmer quenching constant; TSP, sodium trimethylsilylpropionate; RMS, root-mean-squared; 1D, one-dimensional; 2D, two-dimensional; 3D, three-dimensional.

10.1021/bi982159i CCC: $18.00
Published on Web 04/01/1999

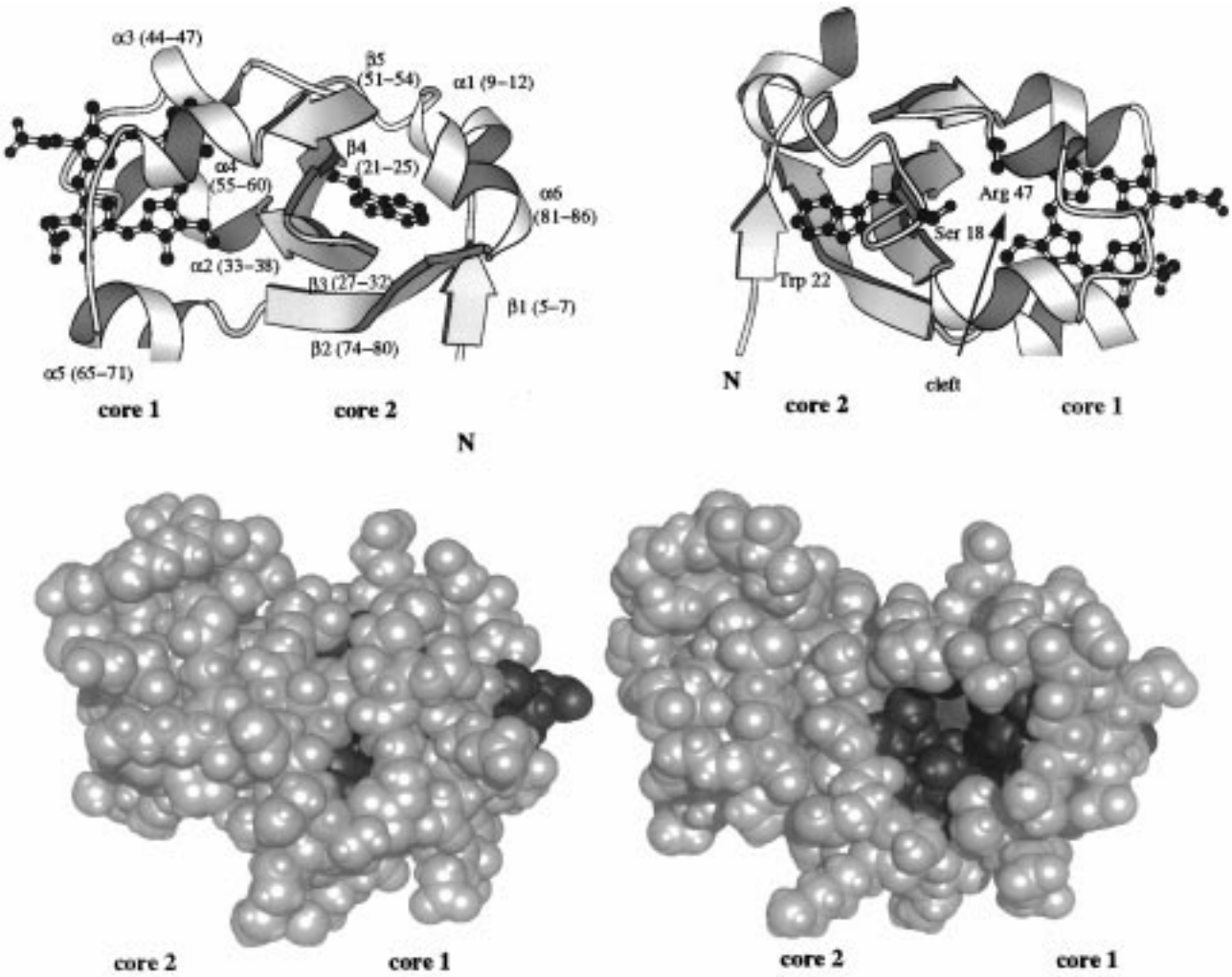

FIGURE 1: Top: Ribbon diagrams of the cyt b_5 crystal structure shown in the 'traditional' orientation (top left) and in a 180° rotated orientation (top right) in order to show the 'cleft' (*52*). The prosthetic heme group, Ser 18, Trp 22, and Arg 47 are shown in black with ball-and-stick. The proposed cleft region lies between Ser 18 and Arg 47. The numbering scheme for bovine cyt b_5 is used. Bottom: Conic representations of the crystal structure and a snapshot from the wild-type MD simulation illustrating the formation of a cleft (*20*). In the 'opened' conformation (bottom right), the hydrophobic core, main chain atoms of Trp 22, and part of the prosthetic heme group are exposed (shown in gray). In the cleft 'closed' conformation (bottom left), these same groups have limited accessibility.

whereas core 2 consists of a β-sheet and two short α-helices. Nearly all of the available mechanistic insight into structure−function relationships of cyt b_5 has been obtained with the cyt b_5−cyt *c* system. Solubilized cyt b_5 forms a functional electron-transfer complex with soluble cyt *c* in vitro (*8*). Numerous approaches have been used to probe the interactions between these partners, and this redox pair has served as a paradigm for interprotein electron transfer. Salemme proposed a static model of the cyt b_5−cyt *c* complex based on X-ray structures of ferric cyt b_5 and ferric cyt *c*, where complex formation is mediated via electrostatic stabilization (*9*). In the model, carboxylate groups of glutamate and aspartate side chains along with a heme propionate on cyt b_5 are 'docked' with complementary lysine and arginine side chains on cyt *c*. The resulting complex yields nearly coplanar heme cofactors. Subsequently, mutagenesis, hyperbaric experiments, and functional studies including measurement of electron-transfer kinetics support the importance of electrostatics in the cyt b_5−cyt *c* interaction (*10*−*15*). Collectively, these studies provide qualitative support for most features of this model. Although individual salt bridges in the complex provide only ∼0.5−1 kcal/mol of stabilization, their collective interactions contribute to the stability and specificity of the complex. The electrostatics, however, provide only 15% of the stabilization energy, suggesting that other types of interactions may be important for complex formation (*14*).

Several experimental and theoretical approaches have been applied to address the role of dynamics within the cyt b_5−cyt *c* complex, and, thereby, to obtain a more refined model. A short MD simulation of the 'Salemme complex' yields a complex with optimized packing at the protein−protein interface, where Fe−Fe distances decreased to an average of 15.7 Å (*16*). Brownian dynamics simulations suggest that the docked complex may be envisioned as an ensemble of complexes with two predominant species (*17, 18*). The dominant interaction predicted by these studies matches well with the 'traditional' cyt *c*−cyt b_5 model. However, the second most populated orientation identified in those simulations requires the cyt *c* to bind to a surface on cyt b_5 that is shifted relative to the 'traditional' surface. In addition, pseudocontact shift NMR studies on the complex also reveal the possibility of multiple binding orientations on the same 'traditional' binding surface (*19*).

The results of a 2.5 ns molecular dynamics (MD) simulation suggest another possible surface for cyt *c* binding (*20*). In the simulation, a patch of surface residues on one face of the molecule is highly dynamic, compared to the remainder of the protein. Specifically, residues contributed from core 1 and core 2 that are close to one another in the X-ray structure transiently move away from each other and then back together, thus restoring the conformation found in the crystal structure (Figure 1). During this process, cyclical formation of a surface cleft exposes the hydrophobic interior including the heme and main chain atoms of Trp 22. Also, several of the acidic residues previously shown to be important for docking with cyt *c* are on the rim of this cleft, and they reorient during the simulation (see Figure 5, *20*). Recent NMR studies (*21*) support the MD results: The molecule is highly dynamic in solution, with redox-state-dependent differences in mobility near the cleft region.

To further test the predictions made on the basis of the MD simulation, site-directed mutants aimed at perturbing cleft dynamics were constructed with a disulfide (S18C:R47C) or salt bridge (S18D), and equilibrium denaturation studies were performed (see accompanying paper, *22*). In those studies, the heme absorbance and fluorescence of the single Trp (Trp 22) were exploited as spectroscopic probes of core 1 and core 2, respectively. Comparison of the thermal denaturation of these proteins indicates that the engineered disulfide or salt bridge has negligible effects on the stability of the protein based on heme absorbance. In contrast, fluorescence changes of Trp 22 consistent with increased solvent accessibility are observed at temperatures well below those required to release heme. Most importantly, the oxidized disulfide mutant (S18C:R47C_{ox}; the subscripts 'ox' and 'red' refer to the oxidation state of the disulfide bond; all studies performed here were with the ferric heme oxidation state) is significantly more stable to temperature-induced changes in Trp 22 fluorescence than either wild type or the S18D mutant. Apparently, the disulfide inhibits or prevents temperature-dependent conformational transitions prior to heme release. At temperatures just below 50 °C, the wild-type protein populates a heme-bound state with fluorescence properties distinct from the native state, and distinct from the disulfide-containing mutant. Although the steady-state fluorescence intensity and spectral shift data are consistent with a temperature-induced change in the local environment of Trp 22 prior to heme release, more detailed characterization is required.

The results from the accompanying paper (*22*) suggest that by inhibiting cleft dynamics, the disulfide bond of S18C:R47C affects the local environment of Trp 22. To directly compare the dynamics surrounding Trp 22 in the wild-type and S18C:R47C proteins, we have utilized steady-state and time-resolved fluorescence quenching, fluorescence anisotropy decay, and ^{1}H NMR at variable temperatures. Together, the results presented here further support the proposal that the dynamics of a 'breathing' motion at the core 1/core 2 interface of cyt b_5 results in transient exposure of a hydrophobic cleft that is restricted in the disulfide mutant.

MATERIALS AND METHODS

Site-Directed Mutagenesis and Protein Purification. Mutagenesis and protein purification protocols of tryptic-solubilized rat cyt b_5 were performed as described in the accompanying paper (*22*). Protein purity was determined by UV−Vis absorbance spectroscopy at a ratio of 280/412 nm of ≤0.18. The purities were verified by SDS−PAGE analysis and MALDI-TOF mass spectrometry (data not shown). The oxidation states of the disulfide mutants, S18C:R47C_{ox} and S18C:R47C_{red}, were determined by susceptibility to carboxymethylation by iodoacetate based on analysis by MALDI-TOF MS (*22*).

Steady-State Fluorescence. Steady-state fluorescence experiments were performed on an SLM-8100 spectrofluorometer using 1 cm quartz cuvettes with stir bars. Temperature was controlled within ±0.4 °C. The excitation was at 295 nm using a detection cutoff filter of 305 nm. The slit widths were 4−8 mm. Samples contained 10 μM cyt b_5 in 5 mM K_2HPO_4 at pH 7. For acrylamide quenching experiments, a 7 M acrylamide stock in 5 mM K_2HPO_4 at pH 7 buffer was used. Blank spectra (buffer only and buffer plus acrylamide) were subtracted from all sample spectra. All spectra reported are the average of at least two emission spectra. The spectral center of mass, λ_{mass}, was determined by integrating the area under the curve from 310 to 370 nm: $\lambda_{mass} = 1/[\sum \nu_i F_i / \sum F_i]$, where F_i is the fluorescence intensity at wavenumber ν_i. Stern−Volmer quenching constants (K_{SV}) were obtained from the relationship (*23*): $F/F_o = 1 + K_{SV}[Q] = 1 + k_q\tau_0[Q]$, where F_o and F are the fluorescence intensities in the absence and presence of quencher, respectively, Q is the acrylamide concentration, and K_{SV} is the Stern−Volmer quenching constant. Also, K_{SV} is equal to $k_q\tau_0$, where k_q is the apparent bimolecular rate constant and τ_0 is the excited-state lifetime in the absence of quencher. We used the average lifetime $\langle\tau\rangle$ at 340 nm to calculate k_q. The apparent rate constant for the quenching reaction, k_q, is equal to γk_d, where γ is the efficiency of the quenching process. Eftink and Ghiron have shown that the efficiency of acrylamide quenching of indole is unity (*24*). Therefore, k_q is equal to k_d, the diffusion-limited rate constant for collisional quenching.

Time-Resolved Fluorescence. Frequency-domain excited-state lifetime and anisotropy measurements were carried out at the Center for Fluorescence Spectroscopy, University of Maryland, Baltimore, MD. Lifetimes were measured with a frequency-domain 10 GHz fluorometer equipped with a Hamamatsu microchannel plate detector (MCP−PMT), described in detail elsewhere (*25*). Excitation was at 295 nm from a mode-locked Ar-ion laser source. Sample emission was filtered through an Oriel interference filter centered at 340 nm. For reference, we used the scatter of the sample solution filtered through an Oriel interference filter at 289 nm with neutral density filters. Samples contained 20 μM cyt b_5 in 5 mM K_2HPO_4 at pH 7.

Data Analysis. The frequency-domain fluorescence phase and modulation data were subject to nonlinear least-squares analysis using the software developed at the Center for Fluorescence Spectroscopy (*26*). Time-resolved intensity decays were described by the multiexponential equation: $I(t) = I_0\sum_i \alpha_i e^{t/\tau_i}$, where $I(t)$ is the emission intensity at time t and I_0 is the initial emission intensity. The amplitude (preexponential factor), α_i, is related to the fraction of molecules in each environment with lifetime τ_i. The measured quantities at each frequency ω, were phase shift, ϕ_ω, and demodulation factor, m_ω, of the emitted light versus a

reference. For anisotropy measurements, the intensities of the parallel and perpendicular anisotropy components at time t are $I_{||}(t) = (1/3)I(t)[1 + 2r(t)]$ and $I_{\perp}(t) = (1/3)I(1 - r(t)]$, respectively, where $r(t)$ is the anisotropy at time t, and $r(t) = r_0\sum_i g_i e^{-t/\phi_i}$. Here, g_i is the amplitude of the ith anisotropy decay component, and ϕ_i is the rotational correlation time of the ith component. The measured quantitites are the phase angle differences between the perpendicular and parallel emission components, $\Delta\phi$, and the amplitude ratio of the parallel and perpendicular components of the modulated emission.

^{1}H NMR Measurements. All NMR experiments were performed on a Varian Inova 500 MHz NMR spectrometer, using a *Z*-axis PFG triple-resonance probe (Varian Inc., Palo Alto, CA). Data were acquired using a gradient-tailored echo sequence (*27*) with a RAW element (*28*) to dephase water. For each experiment, 512 scans were collected with a sweep width of 10 000 Hz and a relaxation delay of 1 s. Data were acquired and processed using VNMR 5.3b software (Varian Inc.). The FIDs were processed with multiplication by a 90° shifted sine bell and zero-filling. Line-broadening of 10 and 4 Hz was applied in the processing of the wild-type and mutant spectra, respectively. The spectra were referenced to TSP, and select resonances were assigned according to ^{1}H NMR assignments made at 40 °C for rat ferric cyt b_5 (*29*). Samples contained 0.5 mM wild type and 1 mM S18C:R47C ferric cyt b_5 in 100 mM Na_2HPO_4 buffer, pH 7.4, in water with 10% D_2O.

RESULTS

Background. In an attempt to alter the dynamics of the putative cleft, S18D and S18C:R47C mutants were designed to favor the 'closed conformation' via a salt bridge or disulfide bond, respectively [Figure 1; also see Figure 2 in accompanying paper (*22*)]. The S18C:R47C mutant was characterized with the disulfide bond oxidized, S18C:R47C$_{ox}$, and reduced and acetylated, S18C:R47C$_{red}$, to examine the cleft in both the 'closed' and 'opened' states. Characterization of the S18C:R47C mutant in the oxidized and reduced forms was done with SDS−PAGE and MALDI-TOF mass spectrometric analysis as described in the accompanying manuscript. The disulfide bond was formed spontaneously, prior to the final purification steps without additional manipulation or oxidation.

Steady-State Fluorescence. The steady-state fluorescence properties of Trp 22 at 25 °C in the wild-type, S18D, S18C:R47C$_{ox}$, and S18C:R47C$_{red}$ proteins have been described in the accompanying manuscript (*22*). Briefly, the wild-type fluorescence spectrum suggests that Trp 22 has a very low quantum yield, with a spectral center of mass (λ_{mass}) at ~340 nm. The relative quantum yields were 1.0, 1.08, 1.06, and 1.01 for wild type, S18D, S18C:R47C$_{ox}$, and S18C:R47C$_{red}$, respectively, based on the emission peak area from 305 to 500 nm, for samples with an absorbance of 0.10 ODU at 295 nm. The relative quantum yields of S18D and S18C:R47C$_{ox}$ were essentially identical to the wild type, but the spectra are blue-shifted modestly (λ_{mass} ~338−339 nm) compared to the wild-type protein. Upon disulfide reduction and acetylation of S18C:R47C, the λ_{mass} red-shifted to 340 nm. These results suggest that Trp 22 in the wild-type and S18C:R47C$_{red}$ proteins was more solvent-exposed than in the S18D or S18C:R47C$_{ox}$ proteins. To further probe the solvent accessibility of Trp 22 in each of these proteins, solute quenching studies were performed with both KI and acrylamide. As expected for a buried Trp, KI was poorly effective as a quencher, and was not used in further experiments (data not shown).

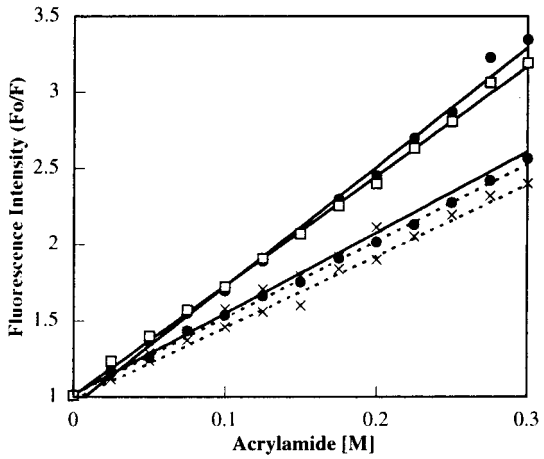

FIGURE 2: Acrylamide quenching of cyt b_5 at 35 °C (dashed lines) and 50 °C (solid lines) for wild type (●), S18C:R47C$_{ox}$ (×), and S18C:R47C$_{red}$ (□). The susceptibility of S18C:R47C$_{ox}$ to acrylamide quenching does not increase with temperature. In contrast, K_{SV} increases significantly for wild type, S18D, and S18C:R47C$_{red}$.

Results for steady-state acrylamide quenching at 5, 35, and 50 °C are summarized in Figure 2 and Table 1. At 5 and 35 °C, each of the proteins exhibited similar sensitivity to quenching by acrylamide. However, at 50 °C modest differences were apparent. Whereas the wild-type and S18D proteins exhibited at least a 2-fold increase in K_{SV} upon raising the temperature, S18C:R47C$_{ox}$ was relatively insensitive. When the reduced disulfide mutant (S18C:R47C$_{red}$) was tested at 50 °C, the K_{SV} was nearly the same value as wild type, suggesting that the oxidized disulfide had closed a route of solvent accessibility to Trp 22. Because the differences between S18C:R47C$_{ox}$ and the other proteins were minimal at 5 and 35 °C, the reduced protein was used only in the 50 °C experiments. As acrylamide concentrations were increased, λ_{mass} blue-shifted as much as 1.7 nm (3 M acrylamide) from the original values. This shift suggested the existence of a heterogeneous population of excited states, where the longer-wavelength-emitting or more solvent-exposed populations were more susceptible to quenching. A likely source of excited-state heterogeneity is ground-state heterogeneity, maintained in the excited state. No curvature of Stern−Volmer plots was apparent in the concentration range of acrylamide used here.

Time-Resolved Fluorescence. Due to limited access to the instrumentation required for the lifetime measurements, time-resolved quenching studies were performed only with the two proteins that exhibited the greatest difference in steady-state quenching, wild type and S18C:R47C$_{ox}$. Also, due to the low intensity of emission for cyt b_5, quenching experiments were performed at a single emission wavelength near the λ_{mass}, 340 nm. The recovered parameters for intensity decay and the collisional quenching constants are summarized in Table 2. Each of the proteins exhibited heterogeneous decay, which was adequately described by a sum of three exponential terms, based on χ^2 values and weighted residuals. At 25 °C, both proteins had similar lifetime

Table 1: Acrylamide Quenching Parameters for Cytochrome b_5

	λ_{mass} (nm)[a]		K_{SV}[b]		
protein	0 M acrylamide	3 M acrylamide	5 °C	35 °C	50 °C
wild type	339.8	338.2	3.69 (0.15)	5.05 (0.08)	7.85 (0.37)
S18D	338.8	337.8	3.46 (0.18)	4.71 (0.02)	7.66 (0.06)
S18C:R47C$_{ox}$	338.5	337.2	2.98 (0.14)	4.04 (0.03)	5.32 (0.31)
S18C:R47C$_{red}$	339.0	NA	NA	NA	7.22 (0.18)

[a] The spectral center of mass was determined as described under Materials and Methods. [b] Stern−Volmer quenching constants were determined as described under Materials and Methods. The numbers in parantheses are standard deviations of the slopes for the linear fits.

Table 2: Fluorescence Lifetime Data Analysis

protein	temp (°C)	$\langle\tau\rangle$ (ns)	τ_1, τ_2, τ_3 (ns)[a]	f_1, f_2, f_3[b]	χ^2	k_q ($\times 10^9$ M^{-1} s^{-1})[c]
wild type	25	3.01	0.08	0.177	1.18	1.68
			1.50	0.301		
			4.88	0.522		
S18C:R47C$_{ox}$		3.60	0.08	0.075	2.96	1.12
			1.37	0.290		
			5.03	0.635		
wild type	50	1.72	0.08	0.261	1.33	4.56
			1.23	0.435		
			3.84	0.303		
S18C:R47C$_{ox}$		2.57	0.09	0.157	1.52	2.07
			1.19	0.358		
			4.40	0.485		

[a] The excited-state lifetimes, τ_i, were calculated from frequency-domain fluorescence phase and modulation data (not shown) as described under Materials and Methods. $\langle\tau\rangle = \sum f_i\tau_i$. [b] Fractional normalized intensities $f_i = \alpha_i\tau_i/\sum\alpha_i\tau_i$. [c] Bimolecular rate constant for acrylamide quenching was calculated using $\langle\tau\rangle$ and K_{SV} (see Table 1). For Table 2 and Table 3, the χ^2 values are 'reduced chi-squares' and approach unity with improved fits.

components of approximately 0.08, 1.4, and 4.9 ns. The fractional intensities of the median lifetime components were very similar for wild type and S18C:R47C$_{ox}$ at both 25 and 50 °C (0.29−0.36). However, the wild type exhibited a nearly 2-fold greater fractional intensity for the short-lifetime component than the mutant, which had a larger fractional intensity for the long-lifetime species. At increased temperatures (50 °C), the median and long lifetimes of each protein decreased, while the shortest component remained the same as at lower temperatures. The decrease in average lifetime was consistent with increasing thermal motion on the nanosecond time scale resulting in collisional quenching of Trp 22 by nearby residues and solvent. To explore the basis for the temperature-induced changes in K_{SV} in steady-state experiments, the excited-state lifetimes were also determined in the presence of several concentrations of acrylamide at variable temperature. These experiments yielded k_q, the bimolecular rate constant for collisional encounter between Trp 22 and acrylamide. Quenching rate constants were not determined for the individual lifetime components, and, therefore, the mean lifetimes were used to calculate k_q for the steady-state quenching reaction (Table 2). Upon increasing the temperature from 25 to 50 °C, k_q for the wild type increased nearly 3-fold, while k_q for the cleft 'closed' mutant, S18C:R47C$_{ox}$, exhibited less than a 2-fold increase in the same temperature range. Thus, the difference in sensitivity to acrylamide quenching between the wild type and disulfide-containing mutant observed in the steady-state experiments was directly attributable in part to differences in the frequency of collisional encounter between Trp 22 and acrylamide. Trp 22 in the wild-type protein became more solvent accessible upon raising the temperature while Trp 22 in the disulfide mutant was less temperature sensitive, as indicated by comparison of k_q values.

Time-Resolved Anisotropy. The temperature-dependent dynamics of Trp 22 were directly probed with frequency-domain time-resolved anisotropy measurements. Specifically, the differential phase angles and modulated anisotropies were determined at 25 and 50 °C for the wild type and S18C:R47C$_{ox}$ mutant. The data are shown in Figure 3, and the recovered parameters from a global analysis are summarized in Table 3. Several features of the data are suggestive of differences in dynamics between the two proteins. At 25 °C, both the wild-type protein and the disulfide mutant exhibited a minor contribution from a component associated with a fast rotational correlation time of 80−90 ps (ϕ_1), which presumably reflected local motion of Trp 22. The fractional contribution for this term was at least 2-fold greater for the wild type than for the disulfide-containing mutant. The data in Figure 3 intuitively suggested complex anisotropy decay with multiple components corresponding to significantly different relaxation times. For both proteins, the data fit significantly better to a two-component exponential anisotropy decay versus a single-exponential decay, on the basis of χ^2 and weighted residuals. In fact, χ^2 values were consistently >20 for single-exponential fits (not shown). Inclusion of the second, fast relaxation component (ϕ_1) was required to obtain reasonable fits of the data. At 25 °C, the $\Delta\phi$ of ~5 °C centered at 300 MHz for the wild type clearly reflected a fast rotational relaxation that was less prominent in the disulfide mutant (Figure 3). It may also be significant that the slower rotational correlation time, ϕ_2, which reflected motion of the entire molecule, was modestly longer for the wild type. The slow rotational correlation times were in reasonable agreement with values predicted on the basis of the molecular weight of cyt b_5 and standard values for hydration (Table 3). The fact that this correlation time was longer for wild type than for S18C:R47C$_{ox}$ is consistent with

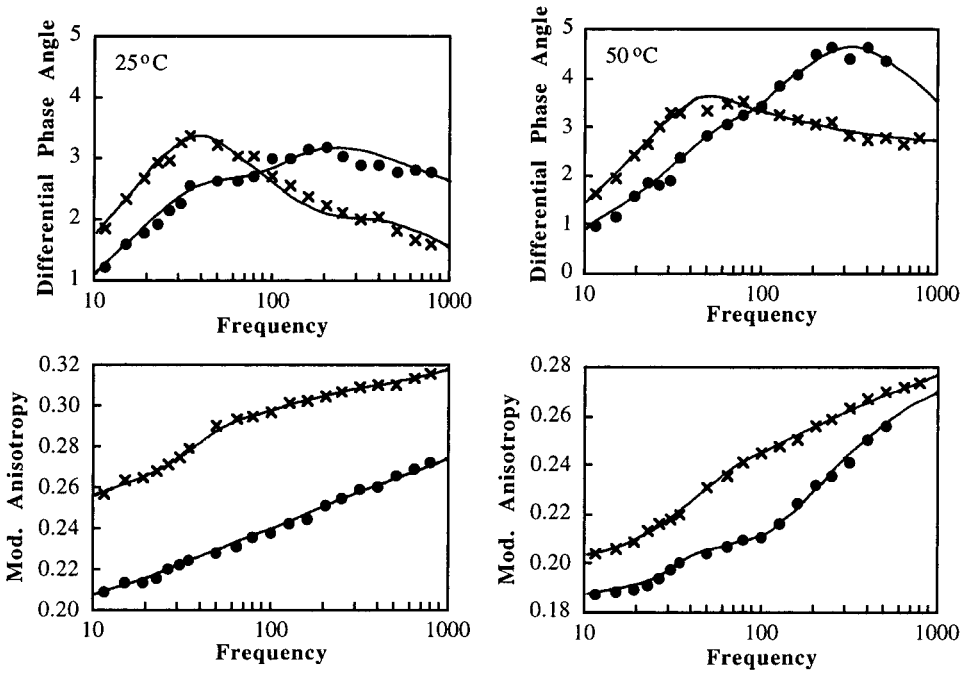

FIGURE 3: Differential phase angles (in degrees) and modulation anisotropy versus frequency for wild type (●) and S18C:R47C$_{ox}$ (×) at 25 °C (left) and 50 °C (right). The frequency scale is in MHz. At both temperatures, the wild type exhibited a larger contribution to anisotropy decay from a 'fast' rotational component with high-frequency response.

Table 3: Time-Resolved Fluorescence Anisotropy Parameters

protein	temp (°C)	r_0[a]	$r_0 g_1$[b]	$r_0 g_2$	ϕ_1 (ns)	ϕ_2 (ns)	predicted ϕ_2[c] (ns)	χ^2
wild type	25	0.235	0.074	0.161	0.09	18.2	5.22	1.4
S18C:R47C$_{ox}$		0.254	0.031	0.223	0.08	14.9	5.21	1.6
wild type	50	0.243	0.115	0.128	0.10	10.1	4.81	1.3
S18C:R47C$_{ox}$		0.243	0.066	0.177	0.07	7.74	4.80	0.8

[a] The limiting anisotropy at zero time. [b] The anisotropy at time t is $r(t) = r_0 g_1 e^{(-t/\phi_1)} + r_0 g_2 e^{(-t/\phi_2)}$, where ϕ_1 and ϕ_2 are the correlation times associated with the components with fractional zero-time anisotropies of $r_0 g_1$ and $r_0 g_2$, respectively. r_0 is the limiting anisotropy at time zero. [c] Predicted value from $r = 3(\mathrm{MW})(\nu + \delta)n/RT$, where MW is the molecular weight of wild type (11 190) or S18C:R47C (11 174), ν is the specific volume of 0.73 mL/g, δ is the hydration state of a globular protein assumed to be 0.4 mL/g, n is 1.004 centipoise, R is the standard gas constant, and T is temperature in degrees kelvin.

a more expanded structure, as would be predicted if a fraction of the molecules were in the 'opened' conformation which is prohibited in the disulfide mutant. At 50 °C, both proteins exhibited an increase in the fractional contribution of the fast rotational component, compared to 25 °C. At the higher temperature, this component remains more prominent in the wild type compared to the disulfide mutant, and in fact is a major source of the anisotropy decay. Taken together, these results support a model in which the surface disulfide bond reduces the local motion of Trp 22 even at increased temperatures.

^{1}H NMR. The solution structures of rat cyt b_5 and other species variants have been well studied through the application of 1D, 2D homo- and heteronuclear, and 3D heteronuclear NMR methods (*29*−*36*). Since a full resonance assignment is beyond the scope of this study, we have restricted our attention to three well-resolved NMR signals that lie between 0.0 and −2.2 ppm on the chemical shift scale, particularly those of Ile 76 δ- and Leu 25 δ'-methyl resonances. Based on location, these residues are good indicators of structural and dynamic changes in cores 1 and 2 of cyt b_5 (Figure 4). Figure 5 shows the upfield region of the 500 MHz ^{1}H NMR spectra for the paramagnetic forms of wild type (panel A) and S18C:R47C$_{ox}$ cyt b_5 (panel B) at 25, 40, and 60 °C. Assignments for the δ'-methyl resonances of Leu 25 and the δ-methyl resonances of Ile 76 were made by comparison of chemical shifts with those published for wild type and mutant rat cyt b_5 at 40 °C (*29, 36*).

Ile 76 δ-Methyl Resonances. The single resonance at −1.19 ppm has been assigned to the δ-methyl protons of Ile 76 in the mutant protein (Figure 5). The chemical shift of these protons was similar but slightly upfield shifted compared to Ile 76 in the wild-type protein (−1.14 ppm) at 40 °C. The pronounced upfield shifts of these protons arise from the fact that they lie above and in van der Waals contact with the indole ring of Trp 22 in core 2 (Figure 4) and hence experience large ring-current shifts. The similarity of the chemical shifts for Ile 76 δ-methyl protons in the mutant and wild-type proteins provided evidence that the structural integrity of core 2 was maintained upon mutagenesis. Due to its isolation from the heme binding core (core 1) of the protein, the chemical shifts of the Ile 76 δ-methyl resonances are relatively unaffected by heme orientation and iron oxidation state as evidenced by the small change in chemical shift (−0.12 ppm) upon change in oxidation state of the metal and the presence of only a single resonance (*29, 34*).

Leu 25 δ′-Methyl Resonances. In contrast to Ile 76, the side chain of Leu 25 lies in core 1, in close proximity to the prosthetic heme group. Thus, chemical shifts of these resonances should indicate structural changes in the heme

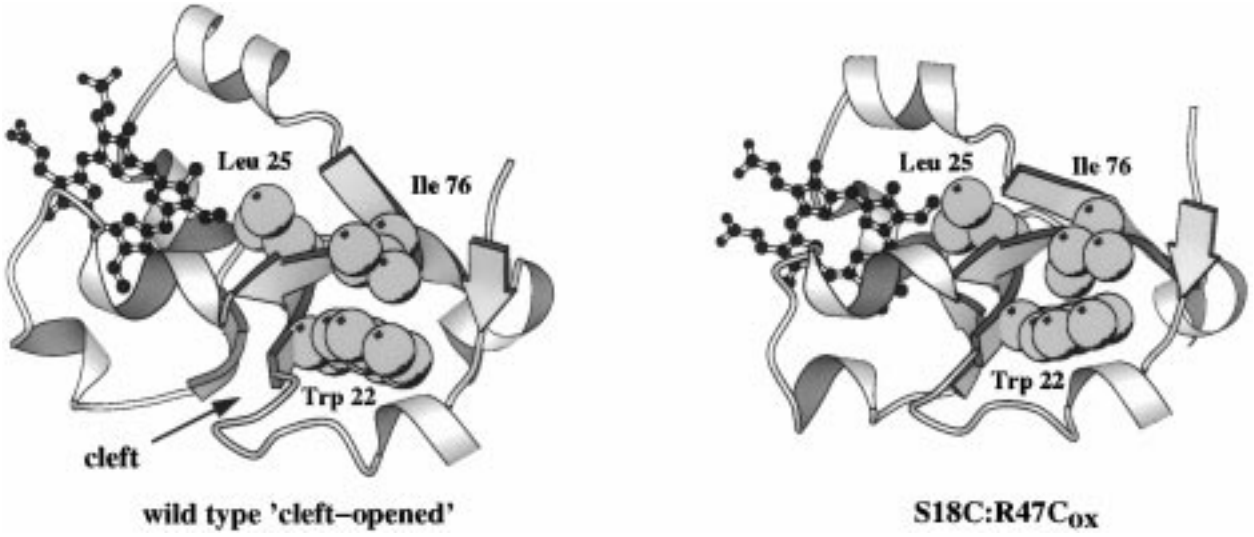

FIGURE 4: Ribbon diagram of cyt b_5 illustrating the locations of Ile 76 and Leu 25 with respect to Trp 22. Leu 25 provides a probe of core 1. Ile 76 is ring-current-shifted by Trp 22 and provides a probe of core 2.

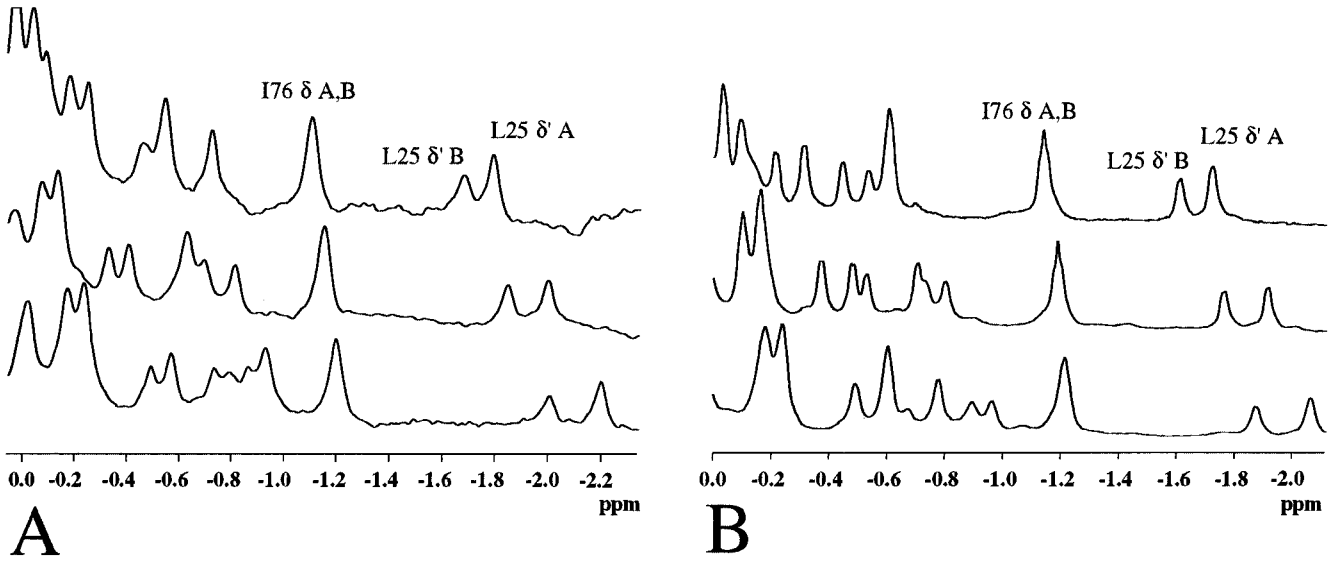

FIGURE 5: Upfield methyl region of the ^{1}H NMR spectra of (A) wild type and (B) S18C:R47C$_{ox}$ cyt b_5 at 25 °C (bottom spectrum), 40 °C (middle spectrum), and 60 °C (top spectrum). Assignment of the upfield methyl resonances of Leu 25 and Ile 76 came from comparison to the published ^{1}H NMR assignments made at 40 °C for the wild-type ferric form of rat cyt b_5 (*29*).

binding region of the protein. The observed chemical shifts for Leu 25 δ'-methyl protons in cyt b_5 are influenced by heme ring-current effects and by the magnitude and orientation of the anisotropic unpaired electron magnetic moment. In addition, doubling of these and other resonances that lie in the vicinity of the heme is due to two equilibrium conformers of cyt b_5 (A and B) that differ in heme orientation (*31*). The resonances at −1.77 and −1.92 ppm have been assigned to the A and B forms of the Leu 25 δ'-methyl protons in S18C:R47C$_{ox}$, respectively. The similarity of these chemical shifts to those determined for the wild-type protein provided strong evidence that the disulfide bridge had not significantly perturbed the structure of the heme binding core. Interestingly, the ratio of peak intensities of the two forms (A:B) is almost 1.2:1 in S18C:R47C$_{ox}$ in contrast to 1.5:1 found for the wild-type protein at 40 °C.

Ile 76 δ-Methyl Resonances as a Probe of Cleft Dynamics. The insensitivity of the Ile 76 δ-methyl resonance to heme effects coupled with its simple identification in 1D 1H NMR spectra makes it an excellent probe of the effect of cleft dynamics on the local environment of Trp 22 in core 2. We measured the chemical shift of the Ile 76 δ-methyl resonance as a function of temperature between 25 and 60 °C, the latter being slightly above the temperature where previous studies have indicated a pronounced difference in structure between wild type and S18C:R47C$_{ox}$ (see accompanying manuscript, *22*). In Figure 6, the chemical shifts of Ile 76 δ-methyl protons are plotted as a function of temperature for mutant and wild-type proteins. Calculated slopes for the wild-type and mutant proteins show that the temperature dependence of the chemical shift is smaller for S18C:R47C$_{ox}$.

DISCUSSION

On the basis of previous results from MD simulations and equilibrium denaturation studies, it was proposed that rationally designed mutations in cyt b_5 should inhibit localized surface dynamics that give rise to the cyclic formation of a cleft (*20, 22*). Furthermore, at increased temperatures prior to heme release, an ensemble of states is obtained in the wild-type protein with an average environ-

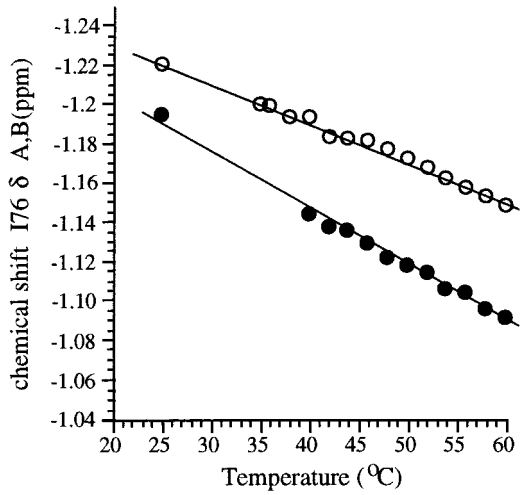

FIGURE 6: Chemical shift versus temperature measured for the δ-methyl group of Ile 76 for wild type (●) and S18C:R47C$_{ox}$ (○). Best linear fits to the data are represented by the solid lines. The wild type is more 'temperature-sensitive' than the S18C:R47C$_{ox}$ mutant.

ment of Trp 22 that is more solvent accessible and dynamic than in the native state. A disulfide mutant designed to close the cleft, S18C:R47C$_{ox}$, does not populate this ensemble of dynamic structures to the same extent as the wild type during urea- or thermal-induced denaturation, or it populates a different conformational space. To support the previous results, Trp 22 was exploited as a probe of dynamics. Here, we have extended and confirmed the model with steady-state and time-resolved fluorescence quenching and fluorescence decay anisotropy as well as variable-temperature 500 MHz ^{1}H NMR. Obviously, the fluorescence and NMR approaches yield dynamic information for very different time scales. It is important to note that, whereas the fluorescence studies may directly provide information concerning the dynamics observed in the MD simulations on the nanosecond time scale in the accompanying manuscript (*22*), the ^{1}H NMR experiments utilized here are not intended as direct probes of motion of Leu-25 or Ile-76. More detailed analysis is required to obtain dynamic NMR parameters for these residues. Rather, the ^{1}H NMR experiments at variable temperature provide information about the relative sensitivity of the local environments of Leu-25 and Ile-76 to temperature. This can only be interpreted as an indirect measure of the dynamics of those local environments.

Cyt b_5 is ideal for the fluorescence studies presented here. It contains a single Trp that is conveniently located near the dynamic cleft area of interest. MD simulations have shown that the backbone of Trp 22 is accessible to solvent through the cleft at the core 1/core 2 interface shown in Figure 1. The side chain of Trp 22 has limited solvent accessibility through core 2. Because of the rigidity of this core even in the apoprotein (*37*−*39*), solvent accessibility through this route should not differ appreciably in the wild-type and mutant proteins, as long as the mutations only affect cleft dynamics at the core 1/core 2 interface.

The steady-state fluorescence spectra of the S18D and S18C:R47C$_{ox}$ mutants are slightly blue-shifted relative to the spectrum of the wild-type protein. The emission spectrum is a direct indicator of local environmental effects on the excited state of the fluorophore. In comparing two proteins, a blue-shifted spectrum may be due to decreased dipolar relaxation around the excited state as a result of decreased solvent accessibility. However, other factors may contribute to spectral shifts, and it is therefore necessary to further probe the physical origins of spectral changes through techniques such as quenching and excited-state lifetime measurements.

The Stern−Volmer analysis of the acrylamide quenching results presented here supported the hypothesis that there is decreased solvent accessibility of Trp 22 in the mutant proteins designed to perturb cleft dynamics. At low temperatures (5 °C), the solvent accessibility of Trp 22 was similar in the wild-type and mutant proteins. As the temperature increased, differences in acrylamide accessibility for each protein became more apparent, presumably due to differential effects on dynamics. At increased temperatures (50 °C), the data suggested that the salt bridge added little to constrain cleft dynamics, resulting in similar Trp accessibility in the S18D and wild-type proteins. The covalent disulfide bond, however, restricted the solvent accessibility of Trp 22 in S18C:R47C$_{ox}$. The results obtained with the reduced disulfide form of the protein were similar to results from wild type and S18D which provided further evidence that the engineered oxidized disulfide bond impeded solvent accessibility of Trp 22.

The time-resolved quenching experiments indicated that the decreased susceptibility of Trp 22 to acrylamide in the disulfide mutant is directly attributable to a decrease in the dynamic quenching rate constant. The recovered k_q increased with temperature for each of the proteins studied, but the disulfide mutant was the least sensitive. Although these experiments provided no structural detail, they demonstrated that Trp 22 is less solvent accessible in the disulfide mutant, as would be predicted from the previous equilibrium denaturation and MD studies in the accompanying paper (*22*). The results also suggested that the hydrophobic cleft was not the only route by which acrylamide quenches Trp 22, as discussed below. If this were the case, then a more pronounced difference between wild type and S18C:R47C$_{ox}$ would be expected. Presumably, Trp 22 is accessible to acrylamide by other routes, and these are not 'closed' by the incorporated disulfide bond or they become accessible in response to strain induced by the disulfide bond. The high degree of Trp accessibility in wild type is supported by the magnitude of the k_q value which approaches the diffusion limit. In fact, k_q values in this range further indicate that cyt b_5 is dynamic and samples conformations other than those observed in the crystal structure.

The rotational correlation times (ϕ_2) measured for the global motion of both wild-type and S18C:R47C$_{ox}$ proteins at 25 and 50 °C were longer than predicted by the Perrin equation for spheres of 'standard' hydration state (*40, 41*). In practice, it is not uncommon to observe rotational correlation times that are ca. 2-fold longer than the predicted values, as is the case here. There are several possible contributions to this increase including deviations from spherical symmetry, large-amplitude motion on the time scale of emission, increased hydration, and alignment of emission dipoles with rotational axes (*42*). In addition, fluorophores with excited-state lifetimes significantly shorter than rotational correlation times are imperfect probes for accurate determination of anisotropy parameters. The average excited-state lifetimes of Trp 22 measured in our experiments

suggested that it was not an ideal probe for the time regime of 5−10 ns. For these reasons, the absolute values of the long correlation times must be viewed qualitatively. However, it is interesting to note that the correlation time associated with the global motion of the protein was longer for the wild type than for the mutant, at both temperatures. We speculate that this may be due to real differences in the shape or hydration of the molecule. For example, the 'opened' conformation expected for the wild type is more elliptical than the 'closed' conformation, with a radius of gyration of ∼12.4 Å, compared to ∼13 Å for the 'closed' conformation of S18C:R47C. This difference can be qualitatively seen when comparing the two proteins in Figures 1 and 4. In the opened conformation, the shortest molecular axis is 19 Å long, and projects through residues 72 and 53. The longest molecular axis is ∼35 Å long and runs nearly parallel to the heme in core 1 and nearly parallel to the indole ring of Trp-22 in core 2, even though the planes of the indole ring and the heme form an angle of ∼40°. This major axis passes through Gly 42 at the surface of core 1 and Asp 82 in core 2. It also runs through the α-carbon of Trp 22. The opened conformation is quite elliptical, with an axial ratio of 1.84. Moreover, it is possible to estimate the angle between the emission dipole of Trp 22 and the long axis of the expanded structure of cyt b_5. The ^1L_a transition dipole of Trp residues dominates the emission at long times after excitation at 295 nm (*43*), and this transition dipole lies within the indole ring at an angle of −38° from the major axis of the indole, and projects through the indole nitrogen. In the 'open' structure of cyt b_5, this vector forms a relatively narrow angle of ∼21° with the longest molecular axis. Thus, the Trp 22 emission dipole and the major axis of rotation are well aligned, and this may contribute to the apparently long ϕ_2 values. It is unlikely that this factor, alone, could cause the correlation time to be 2.5-fold higher than predicted. However, based on the orientation of Trp 22, the molecular asymmetry of cyt b_5 that is enhanced in the 'open' conformation may be nearly fully realized in the anisotropy decay that is due to global motion. Also, the 'opened' conformation provides additional surface area for solvation (∼200 Å^2), and this would contribute to a larger value for the hydration state of the wild type, even though the molecular weight does not change significantly. Therefore, the shorter ϕ_2 correlation times for the disulfide-containing mutant suggested that the hydrodynamic properties of the molecule have been altered, presumably as a result of a decrease in a large-amplitude motion or decrease in hydration.

Of course, a possible explanation for the long rotational correlation times is that cyt b_5 aggregated to form dimers under the conditions of the experiments. In fact, we explicitly looked for the presence of dimers or higher aggregates with gel filtration and nondenaturing gel electrophoresis. We did not observe aggregates, for either wild type or S18C:R47C, under any conditions. Thus, if the proteins were dimers in the fluorescence experiments, the aggregates are not very stable. Even if the proteins were aggregated, then the raw differential phase and modulated anisotropy data (Figure 3) clearly demonstrate a difference in the relative contribution of an anisotropy component with a high-frequency response, that is likely due to a fast local motion of Trp 22, in the wild-type and disulfide-containing mutant. With more detailed NMR studies and analysis of line widths, it should be possible to further probe the possibility of a monomer−dimer equilibrium.

1D ^{1}H NMR methods provide an excellent tool to probe the effects of mutations in localized regions of the proteins. Changes in chemical shifts are often indicators of structural changes (*44*) occurring in a protein as a result of mutation or the binding of a ligand (*45*). While it is difficult to correlate changes in chemical shifts with exact changes in structure, near-identity of chemical shifts can indicate, to a first approximation, structural similarity. In the case of cyt b_5, extensive NMR resonance assignments exist for multiple species variants. Additionally, high-resolution structural information from both X-ray crystallography and NMR is also available. Given this vast body of information, it may be justifiable to correlate structure with chemical shift information derived from 1D ^{1}H NMR data.

As mentioned above, the change in chemical shift of Ile 76 δ-methyl as a function of temperature provides information on the local environment of Trp 22 in core 2. MD simulations of wild-type cyt b_5 indicate that at higher temperatures the cleft undergoes increased thermal fluctuations between 'open' and 'closed' conformations, core 2 becomes more dynamic, and the local structure around Trp 22 is disrupted (see accompanying paper, *22*). The structural perturbations lead to an increase in the average distance between the Ile 76 δ-methyl protons and the Trp 22 indole ring. Consequently, a decreased ring-current effect and concomitant downfield shift occur for these resonances. Figure 6 shows that such an effect is observed in the course of the temperature titration. The smaller downfield shift for the Ile 76 δ-methyl protons over the temperature range indicates that the disulfide bond constrains the cleft to a 'closed conformation'. Interestingly, while the temperature titration of the wild-type protein was found to be completely reversible, that of the mutant protein was irreversible. Comparison of chemical shifts for Ile 76 δ-methyl at 25 °C before and after heating to 60 °C suggests that at higher temperatures S18C:R47C$_{ox}$ was conformationally trapped in local minima and was unable to reequilibrate to the native state due to inhibited cleft mobility.

Structural implications of the inhibition of cleft dynamics on core 1, as reported by Leu 25, are more difficult to interpret on the basis of chemical shifts alone. Differences in observed chemical shifts for wild type and S18C:R47C$_{ox}$ could possibly be due to subtle differences in heme binding orientation and/or orientation of the unpaired electron magnetic moment. Heme binding orientation is strongly influenced by the steric effects of hydrophobic side chain groups in the heme binding pocket. Through systematic investigation of species variants of cyt b_5, LaMar and coworkers conclude that it is the porphyrin rather than the polypeptide that moves to accommodate destabilizing steric interactions caused by varying side chain length of residues in the heme binding pocket (*46*−*49*). Introduction of a disulfide bridge between core 1 and core 2 could have altered side chain packing in the heme binding core, forcing an adjustment by the heme. Fluorescence anisotropy data also indicated that the mutant was more rigid and compact as evidenced by the shorter rotational correlation times, ϕ_2. While the mechanism of the isomer interconversion rate is unknown, it is possible that the mobility of the cleft region

is linked to the dynamics in core 1. While these preliminary results are interesting, a detailed NMR structure and dynamics analysis of the S18C:R47C_{ox} mutant is necessary for any understanding of the influence of cleft dynamics on core 1.

Each of the experimental probes used here, solute quenching, anisotropy decay, and ^{1}H NMR, revealed only modest differences in the dynamic properties or the local environment of Trp 22 upon introduction of the disulfide bond. Together, however, the experimental parameters measured here suggest that altered cleft dynamics caused by the disulfide bond are responsible for the differential temperature effects on each of these probes. Although the cleft provides a major solvent-accessible channel for solute quenchers, and it is the region in which the greatest temperature-dependent changes in structure and dynamics take place, it is not the only region that is affected in the temperature range prior to heme release. Minor increases in dynamics are observed elsewhere, primarily further along the main chain extended from Cys 47 (see accompanying paper, *22*). Therefore, other dynamic modes contribute to solvent accessibility and local motion of Trp 22, and these are not inhibited by the incorporation of the disulfide. In fact, other dynamic modes may be favored when the cleft dynamics are damped. Thus, the disulfide mutant is not completely 'frozen'. However, the engineered disulfide does decrease at least one dynamic mode responsible for local motion and solvent accessibility of core 2 (see Figure 3 in accompanying paper *22*).

ACKNOWLEDGMENT

We thank Michael J. Dabrowski for help in protein purification, Dr. Siddhartha Sarma for suggesting the ^{1}H NMR experiments and for assistance in performing them, and Dr. Ignacy Gryczynski for help with the time-resolved fluorescence experiments and analyses. Brian Bennion is acknowledged for assistance with analysis of the ellipticity. We also acknowledge Zymogenetics, Inc. (Seattle, WA), for the use of their Varian Inova 500 Spectrometer. Figures 1 and 4 were constructed using the Molscript program (*50*). Conic representations in Figure 1 were produced using the MidasPlus program from the Computer Graphics Laboratory, University of California, San Francisco (supported by National Institutes of Health Grant RR-01081) (*51, 52*).

REFERENCES

1. Strittmatter, P., Spatz, L., Corcoran, D., Rogers, M. J., Setlow, B., and Redline, R. (1974) *Proc. Natl. Acad. Sci. U.S.A. 71*, 4565−4569.
2. Okayasu, T., Ono, T., and Shinogima, K. (1977) *Lipids 12*, 267−271.
3. Bernardi, P., and Azzone, G. F. (1981) *J. Biol. Chem. 256*, 7187−7192.
4. Yamazaki, H., Johnson, W. W., Yeng, Y. F., Shimada, T., and Guengerich, F. P. (1996) *J. Biol. Chem. 271*, 27438−27444.
5. Yamazaki, H., Inoue, K., Mimura, M., Oda, Y., Guengerich, F. P., and Shimada, T. (1996) *Biochem. Pharmacol. 51*, 313−319.
6. Katagiri, M., Kagawa, N., and Waterman, M. R. (1995) *Arch. Biochem. Biophys. 317*, 343−347.
7. Auchus, R. J., Lee, T. C., and Miller, W. L. (1998) *J. Biol. Chem. 273*, 3158−3165.
8. Strittmatter, P., and Ozols, J. (1966) *J. Biol. Chem. 241*, 4787−4792.
9. Salemme, F. R. (1976) *J. Mol. Biol. 102*, 563−568.
10. Ng, S., Smith, M. B., Smith, H. T., and Millet, F. (1977) *Biochemistry 16*, 4975−4978.
11. Mauk, M. R., Mauk, A. G., Weber, P. C., and Matthew, J. B. (1986) *Biochemistry 25*, 7085−7091.
12. Mauk, M. R., and Mauk, A. G. (1989) *Eur. J. Biochem. 186*, 473−486.
13. Rodgers, K. K., Pochapsky, T. C., and Sligar, S. G. (1988) *Science 240*, 1657−1659.
14. Rodgers, K. K., and Sligar, S. G. (1991) *J. Mol. Biol. 221*, 1453−1460.
15. Strittmatter, P., Hackett, C. S., Korza, G., and Ozols, J. (1990) *J. Biol. Chem. 265*, 21709−21713.
16. Wendoloski, J. J., Matthew, J. B., Weber, P. C., and Salemme, F. R. (1987) *Science 238*, 794−797.
17. Guillemette, J. G., Barker, P. D., Eltis, L. D., Lo, T. P., Smith, M., Brayer, G. D., and Mauk, A. G. (1994) *Biochimie 76*, 592−604.
18. Moore, G. R., Cox, M. C., Crowe, D., Osborne, M. J., Rosell, F. I., Bujons, J., Barker, P. D., Mauk, M. R., and Mauk, A. G. (1998) *Biochem. J. 332*, 439−449.
19. Guiles, R. D., Sarma, S., DiGate, R. J., Banville, D., Basus, V. J., Kuntz, I. D., and Waskell, L. (1996) *Nat. Struct. Biol. 3*, 333−339.
20. Storch, E. M., and Daggett, V. (1995) *Biochemistry 34*, 9682−9693.
21. Arnesano, F., Banci, L., Bertini, I., and Felli, I. C. (1998) *Biochemistry 37*, 173−184.
22. Storch, E. M., Daggett, V., and Atkins, W. M. (1999) *Biochemistry 38*, 5054−5064.
23. Birks, J. B. (1970) in *Photophysics of aromatic molecules*, pp 433−447, Wiley-Interscience, New York.
24. Eftink, M. R., and Ghiron, C. A. (1976) *Biochemistry 15*, 672−680.
25. Laczko, G., Gryczynski, I., Gryczynski, Z., Wiczk, W., Malak, H., and Lakowicz, J. R. (1990) *Rev. Sci. Instrum. 61*, 2331−2337.
26. Lakowicz, J. R., Cherek, H., Gryczynski, I., Joshi, N., and Johnson, M. L. (1987) *Biophys. Chem. 28*, 35−50.
27. Sklenar, V., Piotto, M., Leppik, R., and Saudek, V. (1993) *J. Magn. Reson., Ser. A 107*.
28. Altieri, A. S., and Byrd, R. A. (1995) *J. Magn. Reson., Ser. B 107*, 260.
29. Guiles, R. D., Basus, V. J., Sarma, S., Malpure, S., Fox, K. M., Kuntz, I. D., and Waskell, L. (1993) *Biochemistry 32*, 8329−8340.
30. Keller, R. M., and Wüthrich, K. (1972) *Biochim. Biophys. Acta 285*, 326−336.
31. LaMar, G. N., Burns, P. D., Jackson, T. J., Smith, K. M., Langry, K. C., and Strittmatter, P. (1981) *J. Biol. Chem. 256*, 5385−5388.
32. Veitch, N. C., Whitford, D., and Williams, R. J. (1990) *FEBS Lett. 269*, 297−304.
33. Guiles, R. D., Altman, J., Kuntz, I. D., and Waskell, L. (1990) *Biochemistry 29*, 1276−1289.
34. Guiles, R. D., Basus, V. J., Kuntz, I. D., and Waskell, L. (1992) *Biochemistry 31*, 11365−11375.
35. Sarma, S., DiGate, R. J., Banville, D. L., and Guiles, R. D. (1996) *J. Biomol. NMR 8*, 171−183.
36. Sarma, S., Dangi, B., Yan, C.-H., DiGate, R. J., Banville, D. L., and Guiles, R. D. (1997) *Biochemistry 36*, 5645−5657.
37. Moore, C. D., Al-Misky, O. N., and Lecomte, J. T. J. (1991) *Biochemistry 30*, 8357−8365.
38. Moore, C. D., and Lecomte, J. T. J. (1990) *Biochemistry 29*, 1984−1989.
39. Moore, C. D., and Lecomte, J. T. J. (1993) *Biochemistry 32*, 199−207.
40. Perrin, F. (1929) *Ann. Phys. 5*, 497.
41. Weber, G. (1952) *Biochem. J. 51*, 145−165.
42. Lakowicz, J. R. (1989) in *Cell Structure and Function by Microspectorfluorometry*, pp 163−183, Academic Press, New York.
43. Gryczynski, Z., Lubkowski, J., and Bucci, E. (1997) *Methods Enzymol. 278*, 540−569.

44. Gao, Y., Veitch, N. D., and Williams, R. J. P. (1991) *J. Biomol. NMR 1*, 457−471.
45. Shuker, S. B., Hadjuk, P. J., Meadows, R. P., and Fesik, S. W. (1996) *Science*, 1531−1534.
46. McLachlan, S. J., LaMar, G. N., and Lee, K.-B. (1988) *Biochim. Biophys. Acta 957*, 430−445.
47. Pochapsky, T. C., Sligar, S. G., McLachlan, S. J., and LaMar, G. N. (1990) *J. Am. Chem. Soc. 112*, 5258−5263.
48. Lee, K.-B., LaMar, G. N., Kehres, L. A., Fujinari, E. M., Smith, K. M., Pochapsky, T. C., and Sligar, S. G. (1990) *Biochemistry 29*, 9623−9631.
49. Lee, K.-B., LaMar, G. N., Mansfield, K. E., Smith, K. M., Pochapsky, T. C., and Sligar, S. G. (1993) *Biochim. Biophys. Acta 1202*, 189−199.
50. Kraulis, P. (1991) *J. Appl. Crystallogr. 24*, 946−950.
51. Ferrin, T. E., Huang, C. C., Jarvis, L. E., and Langridge, R. (1988) *J. Mol. Graphics 6*, 13−27.
52. Huang, C. C., Pettersen, E. F., Klein, T. E., Ferrin, T. E., and Langridge, R. (1991) *J. Mol. Graphics 9*, 230−236.
53. Mathews, F. S., Argos, P., and Levine, M. (1972) *Cold Spring Harbor Symp Quant. Biol. 36*, 387−395.

BI982159I